Chapter 3

SYNTHESIS AND CHARACTERIZATION OF PROPYNYL-TERMINATED Si(111) SURFACES

Plymale, N. T.; Kim, Y.-G.; Soriaga, M. P.; Brunschwig, B. S.; Lewis, N. S. Synthesis, Characterization, and Reactivity of Ethynyl- and Propynyl-Terminated Si(111) Surfaces. *J. Phys. Chem. C* **2015**, *119*, 19847–19862. DOI: 10.1021/acs.jpcc.5b05028

3.1 INTRODUCTION

The chemical composition of semiconductor surfaces can have a substantial impact on the properties of the semiconductor in the context of device architecture.[1-2] The surface composition can drastically influence the rate of charge carrier recombination at the interface,[3-5] the band-edge positions and resulting maximum achievable output potential at the interface,[6-7] the chemical reactivity[8-12] and physical robustness of the interface,[13-14] and the electrical properties of the interface.[15-17] Because the surface composition has such a strong influence over the behavior of semiconductor interfaces, a substantial amount of effort has been put towards achieving molecular-level control over the semiconductor surfaces in order to achieve improved and predictable semiconductor interfaces.

One of the best examples of a well-defined semiconductor surface is methyl-terminated Si(111) (CH_3–Si(111)). As discussed in Chapter 1, CH_3–Si(111) surfaces have been extensively characterized and are believed to be fully-terminated with $–CH_3$ groups such that each atop Si(111) site is terminated by a Si–C bond.[18-33] This property affords CH_3–Si(111) surfaces exceptional chemical stability. This high degree of stability, however, also makes CH_3–Si(111) surfaces chemically inert towards many potential methods of secondary functionalization. Such limitations have precluded CH_3–Si(111) surfaces alone from providing favorable interfaces with functional device components, such as metals, metal oxides, catalysts, and polymers.

Propynyl-terminated Si(111) (CH_3CC–Si(111)) surfaces, which are terminated by the propynyl (–$CCCH_3$) group, could potentially exhibit many properties similar to CH_3–Si(111) surfaces. The –$CCCH_3$ group is sterically similar to –CH_3 groups when considering the radial geometry of the substituent, potentially allowing for near complete termination of the Si(111) atop sites with Si–C bonds. The geometry of the –$CCCH_3$ group is intriguing from a fundamental perspective because it is essentially a –CH_3 group separated from the Si lattice by a C≡C spacer, which presents unique opportunities to improve understanding of organic/Si interactions. Additionally, the propynyl substituent contains a C≡C group, which is synthetically versatile and could allow for facile secondary functionalization of CH_3CC–Si(111) surfaces. In this way, CH_3CC–Si(111) surfaces could also act as an alternative to mixed monolayer chemistry,[10-11, 34] which was developed to allow high Si–C termination on Si surfaces functionalized with bulky, but synthetically useful, alkyl groups by passivating residual halogenated surface sites with –CH_3 groups.

The synthesis of CH_3CC–Si(111) surfaces has been reported previously and extensively cited.[17, 35-39] However, structural characterization of CH_3CC–Si(111) surfaces is severely lacking in the literature, and notable inconsistencies exist between the reported literature preparations and the resulting spectroscopic and physical properties of the surfaces. Further characterization of these surfaces is therefore needed to fully define the functionalization chemistry and to describe the properties of the modified Si(111) surfaces. We describe herein the synthesis of the CH_3CC–Si(111) surfaces and provide extensive characterization of the modified surfaces by transmission infrared spectroscopy (TIRS), high-resolution electron energy-loss spectroscopy (HREELS), X-ray photoelectron spectroscopy (XPS), atomic-force microscopy (AFM), electrochemical scanning-tunneling microscopy (EC-STM), low-energy electron diffraction (LEED), and surface recombination velocity (*S*) measurements. Additionally, we have compared the results of the surface analysis presented herein with previously reported data for propynyl-terminated Si surfaces.

3.2 EXPERIMENTAL SECTION

3.2.1 Materials and Methods

Water (≥18.2 MΩ cm resistivity) was obtained from a Barnstead E-Pure system. Ammonium fluoride (NH_4F(aq), 40%, semiconductor grade, Transene Co., Inc., Danvers, MA) was purged with Ar(g) (99.999%, Air Liquide) for 1 h prior to use.

Czochralski-grown n-Si wafers (Virginia Semiconductor, Fredericksburg, VA) used for the collection of XPS, AFM, EC-STM, LEED, and HREELS data were double-side polished, doped with phosphorus to a resistivity of 1 Ω cm, 381 ± 25 μm thick, and oriented to within 0.1° of the (111) crystal plane. Collection of TIRS data was performed using wafers with one of the following specifications: float-zone-grown n-Si wafers (Silicon Quest International, Santa Clara, CA), double-side polished, doped with phosphorus to a resistivity of 63–77 Ω cm, 435 ± 10 μm thick, and oriented to within 0.5° of the (111) crystal plane; or float-zone-grown Si wafers (Addison Engineering Inc., San Jose, CA), double-side polished, undoped with a resistivity of >20 kΩ cm, 500 ± 20 μm thick, and oriented to within 0.5° of the (111) crystal plane. Undoped, float-zone-grown Si wafers (FZWafers.com, Ridgefield Park, NJ) with a resistivity of 20–40 kΩ cm used for S measurements were double-side polished, 300 ± 25 μm thick, and oriented to within 0.5° of the (111) crystal plane. The wafer thickness was determined using calipers prior to performing S measurements.

1. Preparation of CH_3CC–Si(111) Surfaces. CH_3CC–Si(111) surfaces were prepared from H–Si(111) surfaces using the Cl–Si(111) surface intermediate. Section 2.2.1 of this thesis details the cleaning and etching techniques that were used for the preparation of H–Si(111) surfaces. Cl–Si(111) surfaces were prepared inside a glovebox with <10 ppm O_2(g) by reaction of H–Si(111) surfaces with PCl_5 saturated in chlorobenzene at 90 °C for 45 min using benzoyl peroxide as a radical initiator. A detailed account of the preparation of Cl–Si(111) surfaces can also be found in section 2.2.1.

CH_3CC–Si(111) surfaces were prepared by the reaction of Cl–Si(111) surfaces with CH_3CCLi (1.0 M in hexane, BOC Sciences, Shirley, NY) at 45 ± 2 °C for 3–24 h. The reaction of Cl−Si(111) surfaces with CH_3CCLi was performed in foil-covered test tubes to limit exposure of the CH_3CCLi to ambient light. Upon completion of the reaction,

CH_3CC–Si(111) samples were rinsed with hexanes, then rinsed with and submerged in methanol (≥99.8%, anhydrous, Sigma-Aldrich), removed from the glovebox, sonicated for 10 min in methanol, and rinsed with water. Samples were dried under a stream of Ar(g) or N_2(g). Scheme 3.1 summarizes the preparation methods for CH_3CC–Si(111) surfaces.

Scheme 3.1. Synthesis of CH_3CC–Si(111) Surfaces

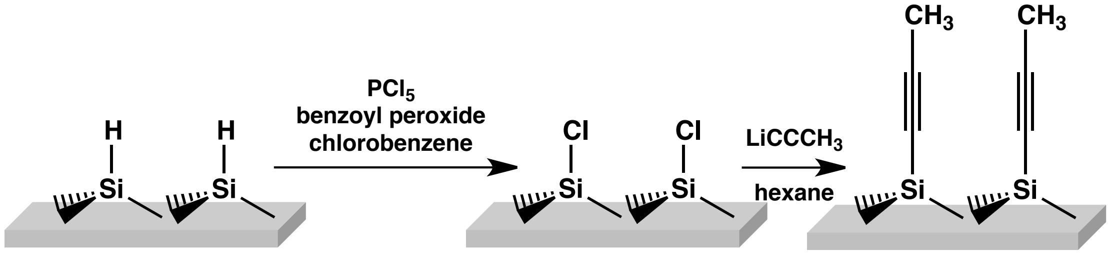

3.2.2 Instrumentation

Detailed descriptions of the instrumentation used in the collection of TIRS, XPS, AFM, EC-STM, LEED, and HREELS data is presented in section 2.2.1.

3.2.3 Data Analysis

1. Fitting and Quantification of XPS Data. High-resolution XP spectra were analyzed using CasaXPS software v. 2.3.16. The fitting parameters were the same as those described in section 2.2.2.

The thickness (d_A) of the overlayer species A was estimated by XPS for CH_3CC–Si(111) surfaces using the substrate-overlayer model[40-41]

$$\left(\frac{I_{\mathrm{A}}}{I_{\mathrm{Si}}}\right)\left(\frac{SF_{\mathrm{Si}}}{SF_{\mathrm{A}}}\right)\left(\frac{\rho_{\mathrm{Si}}}{\rho_{\mathrm{A}}}\right)=\left(\frac{1-e^{\frac{-d_{\mathrm{A}}}{\lambda_{\mathrm{A}}\sin\theta}}}{e^{\frac{-d_{\mathrm{A}}}{\lambda_{\mathrm{Si}}\sin\theta}}}\right) \qquad (3.1)$$

where I_{A} is the area under the photoemission peak arising from the overlayer species A, I_{Si} is the area under the Si 2p photoemission signal, SF_{Si} is the instrument sensitivity factor for Si 2p (0.328), and SF_{A} is the instrument sensitivity factor for the overlayer species A, which is 0.278 for C 1s photoelectrons in hydrocarbon overlayers. For the hydrocarbon overlayers, I_{A} is the total area under the C 1s photoemission signal corresponding to all C atoms in the overlayer, which is composed of the signals at 284.3 and 285.3 eV for CH_3CC–Si(111) surfaces. The density of Si (ρ_{Si}) is 2.3 g cm^{-3}, and the density of the overlayer species A (ρ_{A}) is 3.0 g cm^{-3} for hydrocarbon overlayers.[29] The attenuation length for the overlayer species (λ_{A}) has been estimated to be 3.6 nm for C 1s photoelectrons moving through hydrocarbon overlayers.[42-43] The attenuation length for Si 2p photoelectrons (λ_{Si}) moving through hydrocarbon overlayers has been estimated to be 4.0 nm.[42-43] The angle between the surface plane and the photoelectron ejection vector (θ) is 90°. The thickness of the overlayer species A was calculated using an iterative process.

The fractional monolayer coverage for the overlayer species A (Φ_{A}) was estimated by dividing the measured thickness, d_{A}, by the calculated thickness of 1 ML of overlayer species A, depicted in Scheme 3.2. The thickness of 1 ML of each hydrocarbon overlayer was estimated by summing the bond lengths for the species containing C, but excluding Si and H. Assuming uniform overlayers, the value of Φ_{A} represents the fraction of surface Si(111) sites that were modified with the overlayer species of interest.

Scheme 3.2. Monolayer Thickness of Surface-Bound –$CCCH_3$ Groups

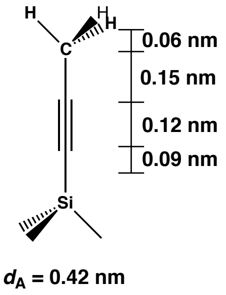

2. Calculation of Surface Recombination Velocity and Surface Trap-State Density. Details on the analysis of surface recombination velocity data for the calculation of S is presented in section 2.2.3. S was calculated for CH_3CC–Si(111) surfaces using eq 2.3.[4] S was converted to a trap state density, N_t, using eq 2.4.[44] N_t was used to estimate the absolute number of electrically active defects per surface Si(111) sites by use of the number density of atop Si sites for an unreconstructed Si(111) surface, $\Gamma_{Si(111)}$, which is 7.83×10^{14} atoms cm^{-2}. Thus, a wafer with surface recombination velocity S has 1 electrically active defect for every $\Gamma_{Si(111)}/N_t$ surface sites.

3.3 RESULTS

3.3.1 Transmission Infrared Spectroscopy

Figure 3.1 shows TIRS data of CH_3CC–Si(111) surfaces. The spectra exhibited three distinct C–H stretching peaks at 2958, 2934, and 2872 cm^{-1}. The absorbance features at 2934 and 2872 cm^{-1} were observed only at the 74° incidence angle, which indicated that those features arose from modes perpendicular to the surface, whereas the absorbance at 2957 cm^{-1} was observed at both angles and was therefore not perpendicular to the surface. A sharp absorbance at 1380 cm^{-1} attributed to the symmetric C–H bending

(δ_s), or "umbrella," mode was present at 74° incidence but was absent at 30° incidence, which indicated that this mode and the propynyl groups were oriented perpendicular to the surface. A broad and asymmetric absorbance with local maxima at 1061, 1033, and 966 cm^{-1} was also observed at both 74° and 30°, and likely arose from the expected CH_3 rocking motion and subsurface $(Si–O–Si)_{TO}$ motion. The C–C stretching absorption was also expected in this region, but likely contributed minimally to this absorption band due to the symmetric nature of the C–C single bond. The presence of an absorbance in the ~1000 cm^{-1} region at both angles of incidence suggested that the absorption arose primarily from the CH_3 rocking and $(Si–O–Si)_{TO}$ modes because the C–C stretching mode is expected to be oriented perpendicular to the surface.

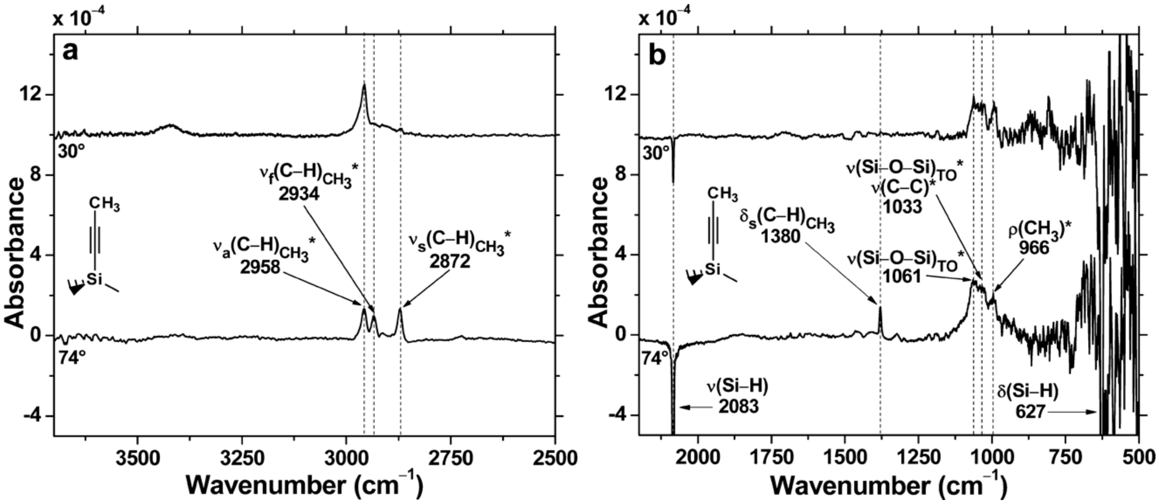

Figure 3.1. TIRS data for $CH_3CC–Si(111)$ surfaces referenced to the H–Si(111) surface collected at 74° (bottom) and 30° (top) from the surface normal. Panel a shows the high-energy region, and panel b shows the low-energy region. The negative peaks in panel b resulted from the H–Si(111) background. The peak positions and assignments (∗ denotes tentative) are indicated in the figure. The 30° spectrum is offset vertically for clarity.

Figure 3.2 shows the absence of detectable Si–H stretching for the CH_3CC–Si(111) surfaces prepared in this work.

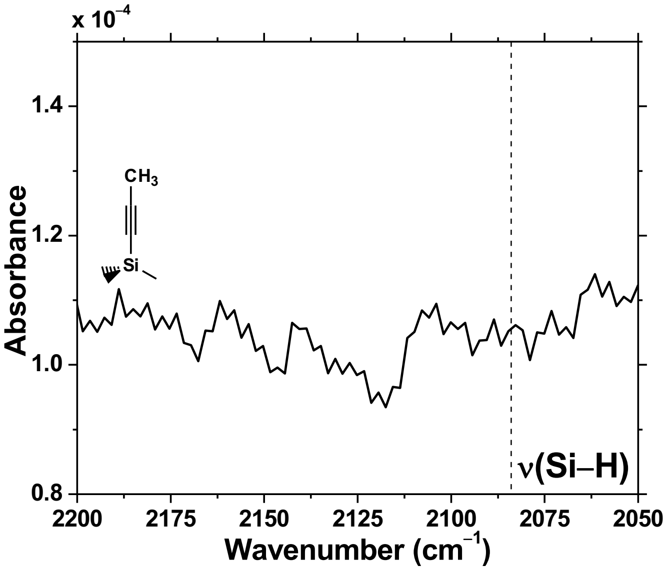

Figure 3.2. TIRS data for the CH_3CC–Si(111) surface referenced to the SiO_x surface. The position of the Si–H stretching peak is indicated by the dotted line.

3.3.2 High-Resolution Electron Energy-Loss Spectroscopy

HREELS data were obtained for CH_3CC–Si(111) surfaces to detect vibrational signals that could not be readily observed by TIRS. The HREELS data for CH_3CC–Si(111) surfaces (Figure 3.3) exhibited a single $(C–H)_{CH_3}$ stretching signal centered at 3004 cm^{-1}, in addition to a broad peak centered at 1435 cm^{-1}, which corresponded to the closely spaced symmetric and asymmetric C–H bending motions, the latter of which was not observed by TIRS. A peak centered at 2216 cm^{-1} was indicative of C≡C stretching, and supported the proposed structure of the CH_3CC–Si(111) surface. A signal at 670 cm^{-1} was consistent with Si–C stretching, and provided evidence for the covalent attachment of propynyl groups to the Si(111) surface. The signal centered at 1048 cm^{-1} arose from the convolution of CH_3 rocking, C–C single-bond stretching, and (Si–O–Si)$_{TO}$ modes.

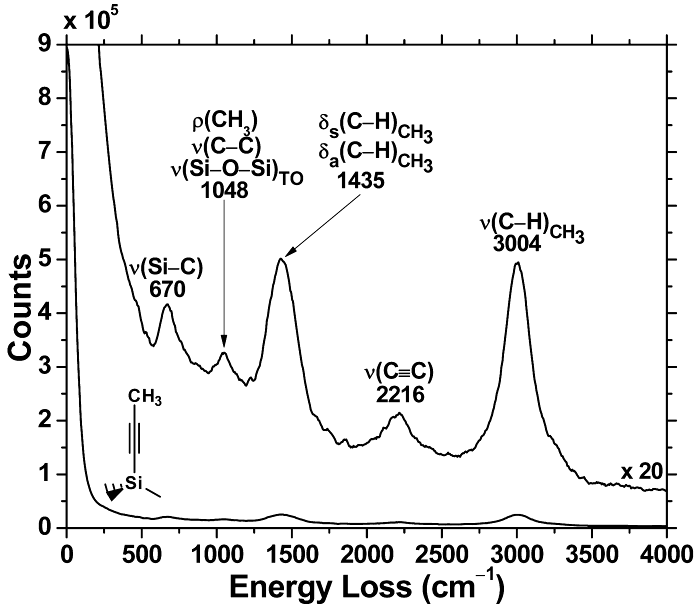

Figure 3.3. HREELS data for CH_3CC–Si(111) surfaces. Data were collected in the specular geometry using an incident beam energy of 2.8 eV, and the fwhm of the elastic peak was 15.0 meV. The raw spectrum (bottom) is shown with the magnified spectrum (top) superimposed for clarity. The peak positions and assignments are indicated in the figure.

Table 3.1 summarizes the vibrational modes observed by TIRS and HREELS for CH_3CC–Si(111) surfaces.

Table 3.1. Summary of the Positions and Assigned Modes for the Vibrational Signatures Observed for CH_3CC–Si(111) Surfaces.

TIRS Frequency (cm^{-1})	**HREELS Frequency (cm^{-1})**[a]	**Assigned Mode**[b]	**Orientation to Surface**[c]
2958	3004	$\nu_a(C{-}H)_{CH_3}*$	not ⊥
2934	3004	$\nu_f(C{-}H)_{CH_3}*$	⊥
2872	3004	$\nu_s(C{-}H)_{CH_3}*$	⊥
–	2216	$\nu(C{\equiv}C)$	
–	1435	$\delta_a(C{-}H)_{CH_3}$	
1380	1435	$\delta_s(C{-}H)_{CH_3}$	⊥
1061	1048	$\nu(Si{-}O{-}Si)_{TO}*$	not ⊥
1033	1048	$\nu(Si{-}O{-}Si)_{TO}*$ $\nu(C{-}C)*$	not ⊥
966	1048	$\rho(CH_3)*$	not ⊥
–	670	$\nu(Si{-}C)$	

[a] In some cases, HREELS signals do not resolve multiple vibrational modes that are observed by TIRS. The HREELS signal with the closest energy to the resolved TIRS signal is paired in the table. [b] The symbols ν, δ, and ρ signify stretching, bending, and rocking motions, respectively, with subscripts a, s, and f indicating whether the mode is asymmetric, symmetric, or resulting from Fermi resonance, respectively. The subscript "CH_3" indicates C–H stretching signals arising from the –CH_3 substituent of the propynyl group. The subscript "TO" indicates a transverse optical Si–O–Si motion. The assignments marked with ∗ are tentative. [c] The orientation of the vibrational mode with respect to the plane of the sample surface determined by TIRS is given.

3.3.3 X-ray Photoelectron Spectroscopy

XPS data were collected to provide quantitative information about the species present on CH_3CC–Si(111) surfaces. Only signals ascribable to Si, C and O were observed, and high-resolution spectra were acquired for the C 1s and Si 2p core levels. Figure 3.4 shows the C 1s high-resolution XP spectrum for CH_3CC–Si(111) surfaces. The C 1s spectra exhibited two distinct photoemission signals centered at 284.3 and 285.3 eV along with a small shoulder centered at 286.6 eV. The low binding-energy peak at 284.3 eV was consistent with C bound to Si, and the prominent photoemission signal at 285.3 eV arose from C bound to C, consistent with the proposed structure of the CH_3CC–Si(111) surface. The signal at 285.3 eV exhibited a broad fwhm relative to the peak at

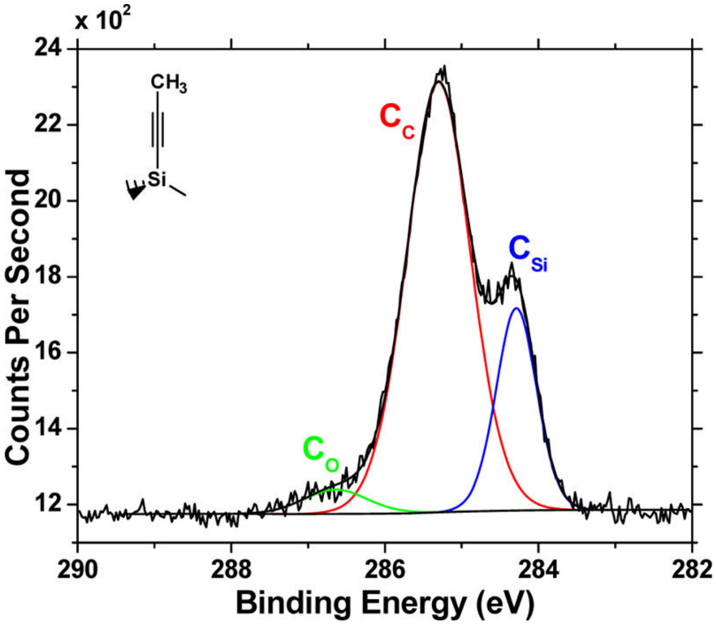

Figure 3.4. High-resolution XP spectrum of the C 1s region for CH_3CC–Si(111) surfaces. The low binding energy C photoemission signal at 284.3 eV arises from C bound to Si (blue, C_{Si}), while the peaks at 285.3 and 286.8 eV arise from C bound to C (red, C_C) and C bound to O (green, C_O), respectively. The peak at 285.3 eV is a convolution of the two C atoms in the propynyl group not bound directly to Si and adventitious C species, while the signal at 286.8 eV arises from adventitious species only.

284.3 eV because the signal at 285.3 eV arose from two chemically different C species in the ≡C–CH_3 substituent of the propynyl moiety as well as adventitious C, while the peak at 284.3 eV arose only from the C bound to Si. The signal centered at 286.6 eV was consistent with adventitious C on alkyl-terminated Si surfaces. The ratio of the peak at 285.3 eV to the peak at 284.3 eV was 3.6 ± 0.4, while, assuming negligible attenuation, the expected ratio for a –$CCCH_3$ group would be 2.0. Figure 3.5 shows the Si 2p high-resolution XP spectrum for CH_3CC–Si(111) surfaces. The spectra showed no detectable SiO_x.

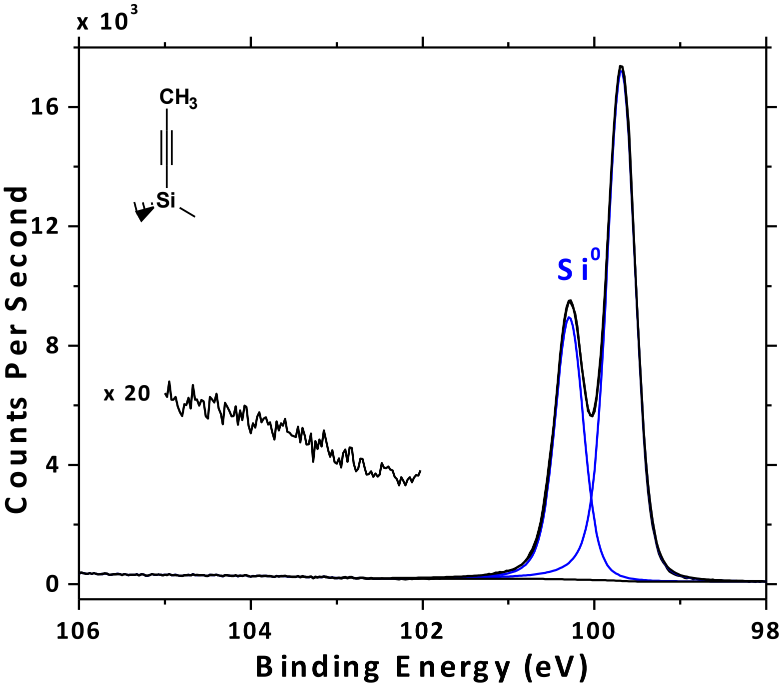

Figure 3.5. High-resolution XP spectrum of the Si 2p region for CH_3CC–Si(111) surfaces. The Si 2p spectrum showed only a contribution from the bulk Si (blue, Si^0). The region from 102–105 eV in the Si 2p spectrum is magnified to show the absence of detectable high-order SiO_x.

The fractional monolayer coverage was estimated for CH_3CC–Si(111) surfaces by XPS by use of eq 1.1[40-41] to yield $\Phi_{\text{Si–CCCH}_3} = 1.05 \pm 0.06$ ML. The C 1s photoemission signals at 284.3 and 285.3 eV were summed to quantify $\Phi_{\text{Si–CCCH}_3}$ because these signals arise directly from the propynyl group. No detectable signals ascribed to Cl, Li, or SiO_x were observed by XPS on CH_3CC–Si(111) surfaces, and XP survey spectra showed very low amounts of O overall.

The thermal stability of CH_3CC–Si(111) surfaces was investigated in vacuum. Figure 3.6 shows the behavior of CH_3CC–Si(111) surfaces as a function of annealing temperature. CH_3CC–Si(111) surfaces exhibited minimal changes in C 1s signal intensity and shape after annealing to 100 °C, with a small reduction in C 1s signal intensity observed upon heating to 200 °C. Annealing to 300 °C produced a significant reduction in the C 1s signal intensity and concomitant reduction in the coverage of Si(111) surface sites by propynyl groups (Table 3.2). Heating to 400 and 500 °C, respectively, further reduced the intensity of the C 1s signal and increased the intensity of the Si 2p signal, indicating that propynyl groups had been desorbed from the Si(111) surface. Annealing the CH_3CC–Si(111) surface up to 500 °C did not change the ratio of the C 1s peak at 285.3 eV to the peak at 284.3 eV within the statistical error, suggesting that very little adventitious C was on the surface. Annealing to 600 °C resulted in increased intensity and broadening of the C 1s signal with the appearance of a new peak centered at ~283.7 eV, which increased in intensity upon further heating to 700 °C and indicated the formation of silicon carbide (SiC).[45-47] An overall increase in the area of the C 1s peak accompanied the formation of SiC and resulted in attenuation of the underlying Si 2p

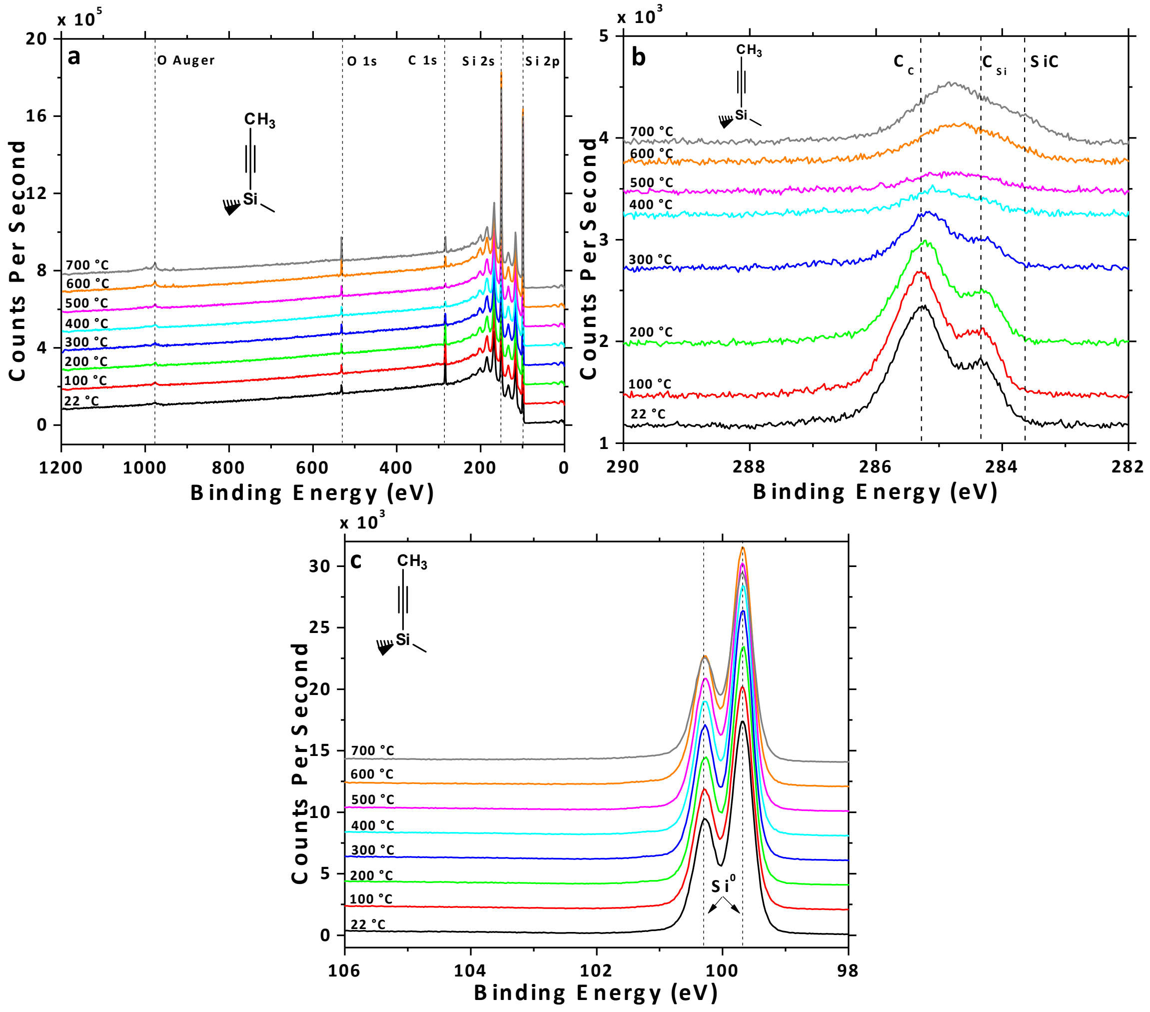

Figure 3.6. Thermal stability in vacuum of CH_3CC–Si(111) surfaces. The annealing temperature is indicated above each spectrum, and the spectra are offset vertically for clarity. The survey spectra (a) show the presence of only the Si 2p, Si 2s, C 1s, and O 1s core level peaks along with the O Auger signal and Si plasmon-loss features. Annealing to 600 and 700 °C resulted in the observation of a small amount of Cu and Cl, which was likely transferred from the sample holder to the sample surface during annealing. The high-resolution C 1s spectra (b) showed the behavior of the C bound to Si (C_{Si}) and C bound to C (C_C) peaks with temperature. Upon annealing to 200–500 °C, the overall amount of C decreased. Heating to 600–700 °C resulted in the appearance of a new C 1s peak at ~283.7 eV (SiC). Si 2p spectra (c) showed increased intensity as C was removed from the surface upon annealing to 500 °C, and decreased intensity upon annealing to 600–700 °C.

photoemission intensity. The chemical structure of the other C species formed on the surface was not readily determined by the XPS measurements performed. Annealing to 600 and 700 °C, respectively, also produced an increase in the O 1s intensity observed in the survey scan, since oxygen-containing hydrocarbon species from the chamber were bound to the surface at elevated temperature.

Table 3.2. The Estimated Fractional ML Coverage, Φ, of a CH_3CC–Si(111) Surface as a Function of Annealing Temperature.

Annealing Temperature (°C)	$\Phi_{Si-CCCH_3}$[a]
22	0.97
100	0.99
200	0.76
300	0.40
400	0.20
500	0.15

[a]The values of Φ were determined using eq 3.1.[40-41] The appearance of SiC on both surfaces upon annealing to 600 °C precluded accurate determination of Φ beyond 500 °C.

3.3.4 Atomic-Force Microscopy, Electrochemical Scanning-Tunneling Microscopy, and Low-Energy Electron Diffraction

Figure 3.7 presents a topographical AFM image of a CH_3CC–Si(111) surface. CH_3CC–Si(111) surfaces exhibited broad atomic terraces with step edges ~0.3 nm in height, consistent with terraces observed on reconstructed Si(111) surfaces in vacuum.[48] Some small particulates were observed on the surfaces, and the amount and size of the particles varied between samples. Since no residual metal or halogen contaminants were detected by XPS on these samples, the particulates were likely organic contaminants. The observation of atomic terraces after alkylation was consistent with the grafting of an overlayer with uniform thickness onto the surface of the Si(111) substrate.

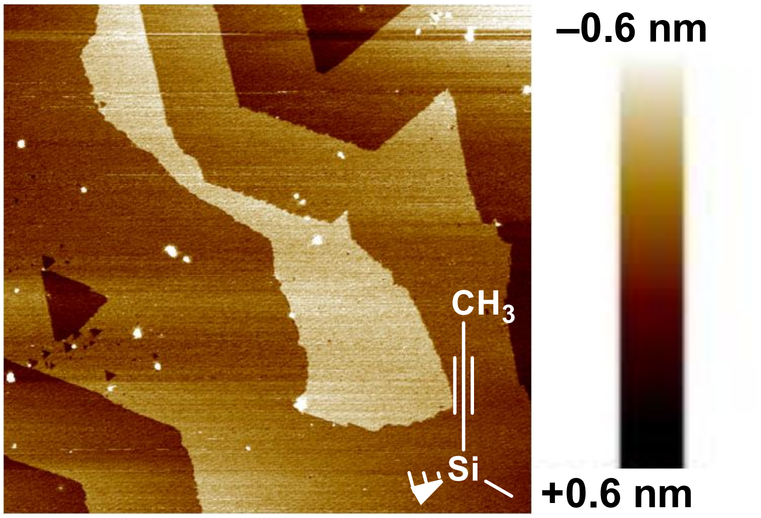

Figure 3.7. Topographical AFM image of a CH_3CC–Si(111) surface. The image is 1 μm × 1 μm with a z-scale of 1.2 nm (–0.6 to +0.6 nm).

Figure 3.8 shows a representative EC-STM image of a CH_3CC–Si(111) surface. CH_3CC–Si(111) surfaces showed localized areas in which some ordering was detectable by room temperature EC-STM. Representative areas in which species of similar height were observed are indicated by white circles, and the distance between the centers of these areas was 0.38 nm, consistent with the distance between Si(111) atop sites.[33] The height variation from the dark to light regions on a single terrace in was 0.08 ± 0.01 nm, which is smaller than the 0.3 nm Si(111) terrace height. The small height variation suggested that the Si substrate was disordered during the grafting process or that species other than CH_3CC–Si(111) groups were present on the surface.

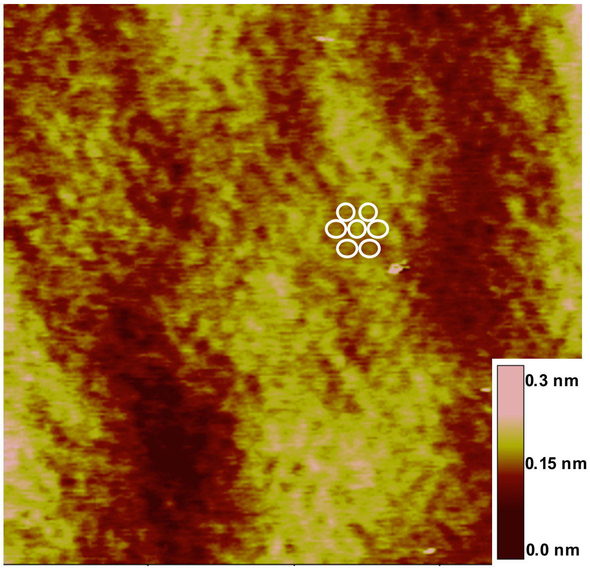

Figure 3.8. Representative EC-STM image a CH_3CC–Si(111) surface (10 nm × 10 nm) collected at –0.4 V versus Ag/AgCl with a bias voltage of –350 mV and tunneling current of 5 nA. The z-scale is indicated in the figure. The white circles in the figures highlight areas where species of similar height were observed, and localized areas of the CH_3CC–Si(111) surface exhibited a (1 × 1) surface unit cell. The distance between the centers of the white circles was 0.38 nm, the same as the distance between Si(111) atop sites.

LEED patterns were collected for CH_3CC–Si(111) surfaces (Figure 3.9) to qualitatively determine the ordering of the top surface layers of the substrate. LEED patters that exhibit 3-fold symmetry indicate a (1 × 1) surface unit cell. However, while LEED is significantly more surface-sensitive than X-ray diffraction, sharp LEED patters are often observed for crystalline samples terminated by a disordered monolayer. The intensity of the background relative to the diffraction spots can qualitatively assist in determining the level of ordering on the surface LEED patterns of CH_3CC–Si(111) surfaces exhibited 3-fold symmetry with the presence of a hexagonal diffraction pattern at 40 eV beam energy, consistent with a (1 × 1) surface unit cell. The intensity of the background was on the same order as that observed for HCC–Si(111) surfaces (see

Chapter 2), which indicated a similar level of ordering at the surface. While both CH_3CC–Si(111) and HCC–Si(111) surfaces exhibited comparably bright and sharp diffraction spots, and the only evidence of lower ordering was in the intensity of the background. Both CH_3CC–Si(111) and HCC–Si(111) surfaces exhibited brighter backgrounds relative to the diffraction spots compared with CH_3–Si(111) surfaces, indicating that the level of surface ordering present on CH_3CC–Si(111) and HCC–Si(111) surfaces was not as long-range as has been found for CH_3–Si(111) surfaces.

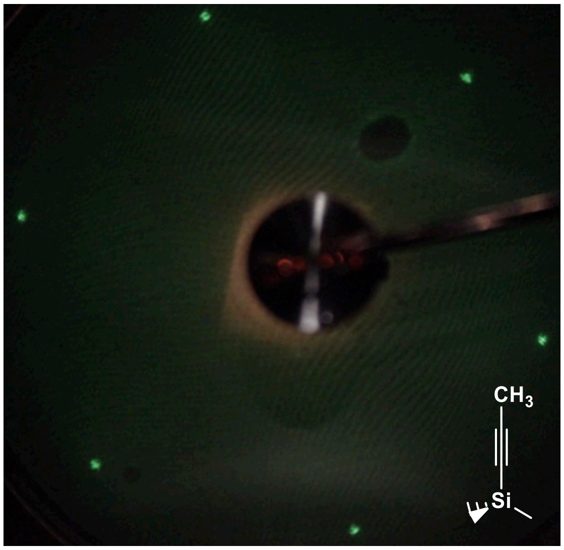

Figure 3.9. Representative LEED pattern for a CH_3CC–Si(111) surface collected at 40 eV incident beam energies.

3.3.5 Surface Recombination Velocity Measurements

Figure 3.10 shows the behavior of *S* determined by use of eq 2.3[4] for CH_3–Si(111) and CH_3CC–Si(111) surfaces as a function of time in air. Immediately after preparation and cleaning, CH_3–Si(111) and CH_3CC–Si(111) surfaces exhibited *S* values of $(4 \pm 2) \times 10^1$ and $(2.0 \pm 0.2) \times 10^3$ cm s^{-1} respectively. After being exposed to air for 24 h, the *S*

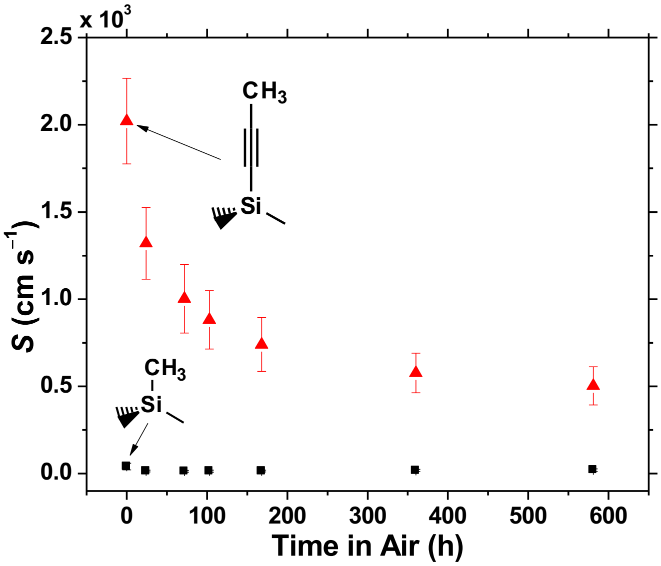

Figure 3.10. *S* measured as a function of exposure to air for CH_3–Si(111) (black squares) and CH_3CC–Si(111) (red triangles) surfaces. The error bars represent 1 standard deviation about the mean.

value for CH_3–Si(111) and CH_3CC–Si(111) surfaces decreased to (1.5 ± 0.5) × 10^1 and (1.3 ± 0.2) × 10^3 cm s^{-1}, respectively. Over extended exposure to air, the *S* value of CH_3CC–Si(111) surfaces continued to decrease, reaching (5 ± 1) × 10^2 cm s^{-1} after 581 h of air exposure.

The effective trap-state density, N_t, was calculated for CH_3–Si(111) and CH_3CC–Si(111) surfaces by use of eq 2.4.[44] Immediately after preparation, CH_3–Si(111) and CH_3CC–Si(111) surfaces were found to have trap-state densities of 4 × 10^9 and 2 × 10^{11} cm^{-2}, which is equivalent to 1 trap for every 2 × 10^5 and 4 × 10^3 surface sites, respectively. After 581 h of exposure to air, the trap-state densities of CH_3–Si(111) and CH_3CC–Si(111) surfaces had adjusted to yield 2 × 10^9 and 5 × 10^{10} cm^{-2}, or 1 trap for every 4 × 10^5 and 2 × 10^4 surface sites, respectively. The estimated trap-state density for the studied surfaces was below the detection limit for most spectroscopies, hindering the identification of the chemical structures that form the surface trap states. However, among CH_3–Si(111), HCC–Si(111) (see Chapter 2), and CH_3CC–Si(111) surfaces, an increased calculated surface coverage of Si−C correlated with decreased S after 581 h of air exposure.

3.4 DISCUSSION

3.4.1 Vibrational Spectroscopy of CH_3CC–Si(111) Surfaces

TIRS (Figure 3.1) and HREELS (Figure 3.3) of CH_3CC–Si(111) surfaces showed vibrational signatures characteristic of the proposed Si–C≡C–CH_3 structure. The polarized "umbrella" mode at 1380 cm^{-1} is significantly higher in energy than the "umbrella" signature that is observed on CH_3–Si(111) surfaces at 1257 cm^{-1}, and this observation is supported by theoretical calculations, which place the CH_3CC–Si(111) "umbrella" mode at ~1392 cm^{-1}.[49] The significant shift in energy is thought to result from the change in bonding environment around the –CH_3 group, which is bonded to either Si or C for CH_3–Si(111) or CH_3CC–Si(111) surfaces, respectively.

Additionally, the CH_3 rocking mode for CH_3CC–Si(111) surfaces at 966 cm^{-1} exhibited a significant shift to higher energy compared with the CH_3 rocking mode for CH_3–Si(111) surfaces at 753 cm^{-1}. The –CH_3 group on the CH_3CC–Si(111) surface is positioned farther from the Si lattice than in the case of CH_3–Si(111) surfaces, resulting in reduced strain and increased energy of the CH_3 rocking motion. This observation is supported by theoretical calculations, which have predicted the appearance of the CH_3

rocking mode at 1018 cm^{-1}.[49] Theory also predicts a C–C stretching mode at approximately 1030 cm^{-1}, but the symmetry of this bond precludes its observation by TIRS. The proximity of this mode to the $(Si–O–Si)_{TO}$ mode as well as to the CH_3 rocking mode yielded a single peak at 1048 cm^{-1} in the HREEL spectrum, preventing the clear observation of the C–C bond by vibrational spectroscopy.

Unlike CH_3–Si(111) surfaces, which exhibit two C–H stretching modes, CH_3CC–Si(111) surfaces show three distinct C–H stretching peaks. Group theory considerations require that a $–CH_3$ group has both a_1 symmetric and e asymmetric C–H stretching modes. However, gas-phase propyne is known to exhibit an absorbance that arises from Fermi resonance between the asymmetric C–H bending (IR inactive) and symmetric C–H stretching modes.[50-51] The a_1 symmetric C–H stretch is expected to have a transition dipole along the axis perpendicular to the surface plane, while the e asymmetric C–H stretch is expected to have a transition dipole parallel to the surface plane. The peak resulting from Fermi resonance is predicted to be centered near twice the energy of the asymmetric C–H bend, which theoretical investigations have estimated to be at 1449 cm^{-1}.[49] A tentative assignment of the C–H stretching peaks from high to low wavenumber is the asymmetric C–H stretch at 2957 cm^{-1}, the Fermi resonance overtone at 2933 cm^{-1}, and the symmetric C–H stretch at 2872 cm^{-1}.

3.4.2 Surface Ordering, Stability, and Defects of CH_3CC–Si(111) Surfaces

CH_3CC–Si(111) surfaces exhibited AFM images that indicated atomically smooth surfaces, and LEED patterns were consistent with a (1 × 1) surface unit cell. However, room temperature EC-STM images of CH_3CC–Si(111) surfaces showed that these surfaces did not exhibit the same long-range ordering characteristic of CH_3–Si(111) surfaces. Instead, localized regions of ordering were observed on CH_3CC–Si(111) surfaces. CH_3CC–Si(111) surfaces exhibited larger regions of uniform coverage compared to HCC−Si(111) surfaces (see Chapter 2), but both surfaces exhibited small variations in height that were not consistent with the height of a Si(111) step edge. For CH_3CC–Si(111) surfaces, the bright and dark regions in Figure 3.8 correspond to ~0.7 ML and ~0.3 ML, respectively. The small difference in height observed between regions was indicative of a difference in the density of states, which could result from a difference in orientation of the $–CCCH_3$ groups or a difference in chemical species bound to the surface. XPS surface coverage estimates predict near complete termination of CH_3CC–Si(111) surfaces with Si–C bonds. Thus, the EC-STM images for CH_3CC–Si(111) surfaces show either regions in which the atop Si atoms were disordered by the functionalization method to yield regions in which the $–CCCH_3$ groups were not normal to the surface, or hydrocarbon impurities were present in the alkylating solution and attached along with the propynyl groups. The height difference on the same terrace was small (<0.1 nm), and the surfaces exhibited localized regions in which ordering was evident, but significant long-range ordering was not observed for CH_3CC–Si(111) surfaces. Given the irreversible nature of the Si–C bond, and the resulting lack of mobility of the surface-bound organic groups, steric considerations could preclude facile formation of a fully ordered alkylated monolayer over large areas, and the ordering observed for CH_3–Si(111) and CH_3–Ge(111) surfaces[52] are thus unique in this respect.

The behavior of the trap-state density as a function of time for CH_3CC–Si(111) surfaces correlates with that observed for CH_3–Si(111) surfaces (see Chapter 1). CH_3–Si(111) surfaces exhibit unusually low trap-state densities that has been attributed to near 1 ML monolayer Φ_{Si-C} and long-range ordering of the surface made possible by the small size of the –CH_3 group. The CH_3CC–Si(111) surface has a thicker carbon overlayer and higher Φ_{Si-C} compared with the HCC–Si(111) surface (see Chapter 2). These characteristics better protect the CH_3CC–Si(111) surface from oxidation and ultimately afford it a lower overall trap-state density. The decrease in trap-state density with time exposed to air observed for CH_3–Si(111) and CH_3CC–Si(111) surfaces could result from reaction of the existing trap states with water and oxygen in the air without breaking the Si–Si backbonds.

The thermal stability behavior of CH_3CC–Si(111) surfaces indicates that CH_3CC–Si(111) surfaces have a lower thermal stability than CH_3–Si(111) surfaces, which are known to be stable up to 450 °C in vacuum.[45, 53] CH_3CC–Si(111) surfaces appeared to show a loss of the propynyl groups as the sample was annealed to 300–500 °C because the overall intensity of the C 1s peak decreased. The desorption of –$CCCH_3$ groups from the sample surface is comparable to the behavior observed for H_5C_2–Si(111) surfaces, which exhibit ~40% reduction in C bound to Si upon annealing to 300 °C.[45] Formation of SiC on CH_3CC–Si(111) surfaces annealed to 600 and 700 °C, respectively, was limited by the reduced amount of C on the surface after annealing. These results suggest that the –$CCCH_3$ surfaces are hindered from reacting with hydrocarbons in the vacuum chamber by the –CH_3 group, and the Si–C bond breaks before the C≡C bond can react. The results indicate that the Si–C bond is destabilized for organic species containing Si–C≡C–R functionality compared with CH_3–Si(111) surfaces.

3.4.3 Comparison with Previously Reported Syntheses and Surface Spectroscopy

Preparation of CH_3CC–Si(111) surfaces has been reported by reaction of Cl–Si(111) surfaces with CH_3CCNa in THF[35] or $CH_3CCMgBr$ in THF.[17, 36-38] Table 3.3 summarizes the synthetic methods, surface characterization techniques employed, and results of the prior studies. Anodic deposition of $CH_3CCMgBr$ on H–Si(111) surfaces has also been reported, but a polymeric layer was formed on the surface.[39] Our attempts to prepare CH_3CC–Si(111) surfaces by the published halogenation/alkylation procedures yielded widely varying results that were not in general agreement with the detailed spectroscopic signatures and results reported herein. Vibrational spectra reported for anodic deposition of $CH_3CCMgBr$ on H–Si(111) surfaces showed the presence of a peak at ~1100 cm^{-1}, which was assigned to a C≡C–C stretching mode[39] and is very near the peaks reported in this work at 1061, 1033, and 966 cm^{-1}. However, due to the polymeric nature of the grafted layer, the modes associated with the CH_3 group of the propynyl moiety were not observed. Using the synthetic routes presented herein, the observation of the vibrational signatures, particularly the C≡C stretch at 2216 cm^{-1}, C–H "umbrella" at 1380 cm^{-1}, and Si–C stretch at 670 cm^{-1}, strongly support the attachment of propynyl groups to the Si(111) surface.

Table 3.3. Summary of Prior Reports of Synthesis and Characterization of Propynyl-Terminated Si Surfaces

Publication	**Reaction Conditions**	**Characterization and Evidence for Structure**
ref[35]	Cl–Si(111) reacted with $NaCCCH_3$ in THF to give Si–$CCCH_3$ surfaces.	XPS: C 1s XP peak at 284.0 eV used to suggest C bound to Si. Coverage estimated to be 1.05 ± 0.1 ML for Si–$CCCH_3$ relative to Si–CH_3. No evidence for SiO_x in Si 2p. Electrochemical measurements show no Si–H oxidation peak in aqueous electrolyte.
ref[17]	Cl–Si(111) reacted with $CH_3CCMgBr$ in THF at 120–130 °C for 24 h to give Si–$CCCH_3$ surfaces.	No structural characterization reported. Electrochemical measurements for Si–$CCCH_3$ surfaces in contact with Hg were shown to exhibit behavior similar to Si–CH_3 surfaces.
ref[38]	Cl–Si(111) reacted with $CH_3CCMgBr$ in THF at 120–130 °C for 27 h to yield Si–$CCCH_3$ surfaces.	XPS: C1s XP peak at 284.0 eV used to suggest C bound to Si. Coverage with –$CCCH_3$ groups was estimated to be 1.05 ± 0.1 ML relative to Si–CH_3. No SiO_x observed after preparation. SiO_x was ~0.5 ML after 24 h in water and ~0.15 ML after 65 days in air. ToF-SIMS showed $SiCH_3^+$ and $SiC_3H_3^+$ fragment peak intensities were in a ratio of ~3:2 for Si–$CCCH_3$ surfaces.
ref[36]	Cl–Si(111) reacted with $CH_3CCMgBr$ in THF at 120–130 °C for 27 h to yield Si–$CCCH_3$ surfaces.	XPS results are similar to those reported in the previous citation. ToF-SIMS raw data is presented, and shows that Si–$CCCH_3$ surfaces gave $SiCH_3^+$ and $SiC_3H_3^+$ (peak ratio 1.9:1) for positive ToF-SIMS. $C_3H_3^-$ and SiO_2 (peak ratio 2.7:1) were the primary peaks for negative ToF-SIMS. Spectroscopic ellipsometry gave a thickness of 5.8 Å for Si–$CCCH_3$ surfaces, in agreement with theory.
ref[37]	Cl–Si(111) and Si–Cl nanowires reacted with $CH_3CCMgBr$ in THF at 120–130 °C for 12–27 h to yield Si–$CCCH_3$ planar or nanowire surfaces, respectively.	XPS: Si nanowires functionalized with –$CCCH_3$ groups exhibit SiO_x/Si bulk 2p area ratio of 0.15 after 720 h of air exposure, which is faster than nanowires functionalized with –CH_3 or –CH=CH–CH_3 groups. However, comparative studies performed on Si(111) surfaces show much slower oxidation for CH_3CC–Si(111) (SiO_x/Si bulk 2p area ratio ~0.07 after 720 h air exposure) surfaces compared with CH_3–Si(111) surfaces.
ref[39]	Anodic grafting of HCCMgCl and HCCMgBr in THF to H–Si(111) surfaces. The current density was 0.5 or 0.02 mA cm^{-2} applied over 15–20 min.	SEM indicated the presence of a polymeric layer for all samples prepared. IR: All samples showed disappearance of Si–H after anodic deposition. Samples prepared from $CH_3CCMgBr$ showed a C≡C–C stretching vibration at ~1100 cm^{-1}, and no C–H stretching peaks were observed. SXPS: A C 1s XP peak at 283.7 eV was used to qualitatively suggest C bound to Si. Si 2p XP spectra showed shift in surface Si to higher binding energy, further suggesting that the surface Si is bound to C.

3.5 CONCLUSIONS

CH_3CC–Si(111) surfaces have been synthesized and characterized by a variety of spectroscopic methods. TIRS and HREELS data show the characteristic vibrational modes for Si–C≡C–CH_3 groups covalently bound perpendicular to the surface. Quantification of XPS data for CH_3CC–Si(111) surfaces exhibited $\Phi_{\text{Si–CCCH}_3} = 1.05 \pm 0.06$ ML. The prepared surfaces exhibited no detectable unreacted Si–H or Si–Cl sites. Annealing of CH_3CC–Si(111) surfaces in vacuum resulted in desorption of the –$CCCH_3$ groups. AFM and LEED data showed that the surfaces exhibited terraced structures and ordering comparable to that of CH_3–Si(111) surfaces, though EC-STM data showed that the surfaces did not exhibit the long-range ordering of CH_3–Si(111) surfaces.

The complete vibrational spectra for the CH_3CC–Si(111) surfaces presented in this work definitively establish the covalent attachment of ethynyl and propynyl groups to the Si(111) surface. The use of a wide range of surface-sensitive spectroscopic and microscopic techniques provides a clear picture of the surface structure, allowing for the development of structure–function relationships and new chemistries. The development of a comprehensive understanding of the chemical and physical properties of synthesized surfaces is of extraordinary importance in order to further the use of monolayer chemistry in the development of novel new semiconductor devices.

3.6 REFERENCES

1. Bent, S. F. Organic Functionalization of Group IV Semiconductor Surfaces: Principles, Examples, Applications, and Prospects. *Surf. Sci.* **2002**, *500*, 879-903.
2. Buriak, J. M. Organometallic Chemistry on Silicon and Germanium Surfaces. *Chem. Rev.* **2002**, *102*, 1271-1308.
3. Gstrein, F.; Michalak, D. J.; Royea, W. J.; Lewis, N. S. Effects of Interfacial Energetics on the Effective Surface Recombination Velocity of Si/Liquid Contacts. *J. Phys. Chem. B* **2002**, *106*, 2950-2961.
4. Royea, W. J.; Juang, A.; Lewis, N. S. Preparation of Air-Stable, Low Recombination Velocity Si(111) Surfaces through Alkyl Termination. *Appl. Phys. Lett.* **2000**, *77*, 1988-1990.
5. Royea, W. J.; Michalak, D. J.; Lewis, N. S. Role of Inversion Layer Formation in Producing Low Effective Surface Recombination Velocities at Si/lLiquid Contacts. *Appl. Phys. Lett.* **2000**, *77*, 2566-2568.
6. Li, Y.; O'Leary, L. E.; Lewis, N. S.; Galli, G. Combined Theoretical and Experimental Study of Band-Edge Control of Si through Surface Functionalization. *J. Phys. Chem. C* **2013**, *117*, 5188-5194.
7. Plymale, N. T.; Kim, Y.-G.; Soriaga, M. P.; Brunschwig, B. S.; Lewis, N. S. Synthesis, Characterization, and Reactivity of Ethynyl- and Propynyl-Terminated Si(111) Surfaces. *J. Phys. Chem. C* **2015**, *119*, 19847-19862.
8. Lattimer, J. R. C.; Blakemore, J. D.; Sattler, W.; Gul, S.; Chatterjee, R.; Yachandra, V. K.; Yano, J.; Brunschwig, B. S.; Lewis, N. S.; Gray, H. B. Assembly, Characterization,

and Electrochemical Properties of Immobilized Metal Bipyridyl Complexes on Silicon(111) Surfaces. *Dalton Trans.* **2014**, *43*, 15004-15012.

9. Lattimer, J. R. C.; Brunschwig, B. S.; Lewis, N. S.; Gray, H. B. Redox Properties of Mixed Methyl/Vinylferrocenyl Monolayers on Si(111) Surfaces. *J. Phys. Chem. C* **2013**, *117*, 27012-27022.
10. O'Leary, L. E.; Rose, M. J.; Ding, T. X.; Johansson, E.; Brunschwig, B. S.; Lewis, N. S. Heck Coupling of Olefins to Mixed Methyl/Thienyl Monolayers on Si(111) Surfaces. *J. Am. Chem. Soc.* **2013**, *135*, 10081-10090.
11. O'Leary, L. E.; Strandwitz, N. C.; Roske, C. W.; Pyo, S.; Brunschwig, B. S.; Lewis, N. S. Use of Mixed CH_3–/$HC(O)CH_2CH_2$–Si(111) Functionality to Control Interfacial Chemical and Electronic Properties During the Atomic-Layer Deposition of Ultrathin Oxides on Si(111). *J. Phys. Chem. Lett.* **2015**, *6*, 722-726.
12. Plass, K. E.; Liu, X.; Brunschwig, B. S.; Lewis, N. S. Passivation and Secondary Functionalization of Allyl-Terminated Si(111) Surfaces. *Chem. Mater.* **2008**, *20*, 2228-2233.
13. Cho, C. J.; O'Leary, L.; Lewis, N. S.; Greer, J. R. In Situ Nanomechanical Measurements of Interfacial Strength in Membrane-Embedded Chemically Functionalized Si Microwires for Flexible Solar Cells. *Nano Lett.* **2012**, *12*, 3296-3301.
14. Gallant, B. M.; Gu, X. W.; Chen, D. Z.; Greer, J. R.; Lewis, N. S. Tailoring of Interfacial Mechanical Shear Strength by Surface Chemical Modification of Silicon Microwires Embedded in Nafion Membranes. *ACS Nano* **2015**, *9*, 5143-5153.

15. Maldonado, S.; Knapp, D.; Lewis, N. S. Near-Ideal Photodiodes from Sintered Gold Nanoparticle Films on Methyl-Terminated Si(111) Surfaces. *J. Am. Chem. Soc.* **2008**, *130*, 3300-3301.
16. Maldonado, S.; Lewis, N. S. Behavior of Electrodeposited Cd and Pb Schottky Junctions on CH_3-Terminated n-Si(111) Surfaces. *J. Electrochem. Soc.* **2009**, *156*, H123-H128.
17. Maldonado, S.; Plass, K. E.; Knapp, D.; Lewis, N. S. Electrical Properties of Junctions between Hg and Si(111) Surfaces Functionalized with Short-Chain Alkyls. *J. Phys. Chem. C* **2007**, *111*, 17690-17699.
18. Bansal, A.; Lewis, N. S. Stabilization of Si Photoanodes in Aqueous Electrolytes through Surface Alkylation. *J. Phys. Chem. B* **1998**, *102*, 4058-4060.
19. Bansal, A.; Lewis, N. S. Electrochemical Properties of (111)-Oriented n-Si Surfaces Derivatized with Covalently-Attached Alkyl Chains. *J. Phys. Chem. B* **1998**, *102*, 1067-1070.
20. Bansal, A.; Li, X.; Lauermann, I.; Lewis, N. S.; Yi, S. I.; Weinberg, W. H. Alkylation of Si Surfaces Using a Two-Step Halogenation/Grignard Route. *J. Am. Chem. Soc.* **1996**, *118*, 7225-7226.
21. Bansal, A.; Li, X.; Yi, S. I.; Weinberg, W. H.; Lewis, N. S. Spectroscopic Studies of the Modification of Crystalline Si(111) Surfaces with Covalently-Attached Alkyl Chains Using a Chlorination/Alkylation Method. *J. Phys. Chem. B* **2001**, *105*, 10266-10277.

22. Becker, J. S.; Brown, R. D.; Johansson, E.; Lewis, N. S.; Sibener, S. J. Helium Atom Diffraction Measurements of the Surface Structure and Vibrational Dynamics of CH_3--Si(111) and CD_3--Si(111) Surfaces. *J. Chem. Phys.* **2010**, *133*, 104705.
23. Brown, R. D.; Hund, Z. M.; Campi, D.; O'Leary, L. E.; Lewis, N. S.; Bernasconi, M.; Benedek, G.; Sibener, S. J. Hybridization of Surface Waves with Organic Adlayer Librations: A Helium Atom Scattering and Density Functional Perturbation Theory Study of Methyl-Si(111). *Phys. Rev. Lett.* **2013**, *110*, 156102.
24. Brown, R. D.; Hund, Z. M.; Campi, D.; O'Leary, L. E.; Lewis, N. S.; Bernasconi, M.; Benedek, G.; Sibener, S. J. The Interaction of Organic Adsorbate Vibrations with Substrate Lattice Waves in Methyl-Si(111)-(1 × 1). *J. Chem. Phys.* **2014**, *141*, 024702.
25. Grimm, R. L.; Bierman, M. J.; O'Leary, L. E.; Strandwitz, N. C.; Brunschwig, B. S.; Lewis, N. S. Comparison of the Photoelectrochemical Behavior of H-Terminated and Methyl-Terminated Si(111) Surfaces in Contact with a Series of One-Electron, Outer-Sphere Redox Couples in CH_3CN. *J. Phys. Chem. C* **2012**, *116*, 23569-23576.
26. Nihill, K. J.; Hund, Z. M.; Muzas, A.; Díaz, C.; del Cueto, M.; Frankcombe, T.; Plymale, N. T.; Lewis, N. S.; Martín, F.; Sibener, S. J. Experimental and Theoretical Study of Rotationally Inelastic Diffraction of $H_2(D_2)$ from Methyl-Terminated Si(111). *J. Chem. Phys.* **2016**, *145*, 084705.
27. Webb, L. J.; Lewis, N. S. Comparison of the Electrical Properties and Chemical Stability of Crystalline Silicon(111) Surfaces Alkylated Using Grignard Reagents or Olefins with Lewis Acid Catalysts. *J. Phys. Chem. B* **2003**, *107*, 5404-5412.
28. Webb, L. J.; Michalak, D. J.; Biteen, J. S.; Brunschwig, B. S.; Chan, A. S. Y.; Knapp, D. W.; Meyer, H. M.; Nemanick, E. J.; Traub, M. C.; Lewis, N. S. High-Resolution

Soft X-ray Photoelectron Spectroscopic Studies and Scanning Auger Microscopy Studies of the Air Oxidation of Alkylated Silicon(111) Surfaces. *J. Phys. Chem. B* **2006**, *110*, 23450-23459.

29. Webb, L. J.; Nemanick, E. J.; Biteen, J. S.; Knapp, D. W.; Michalak, D. J.; Traub, M. C.; Chan, A. S. Y.; Brunschwig, B. S.; Lewis, N. S. High-Resolution X-ray Photoelectron Spectroscopic Studies of Alkylated Silicon(111) Surfaces. *J. Phys. Chem. B* **2005**, *109*, 3930-3937.
30. Webb, L. J.; Rivillon, S.; Michalak, D. J.; Chabal, Y. J.; Lewis, N. S. Transmission Infrared Spectroscopy of Methyl- and Ethyl-Terminated Silicon(111) Surfaces. *J. Phys. Chem. B* **2006**, *110*, 7349-7356.
31. Wong, K. T.; Lewis, N. S. What a Difference a Bond Makes: The Structural, Chemical, and Physical Properties of Methyl-Terminated Si(111) Surfaces. *Acc. Chem. Res.* **2014**, *47*, 3037-3044.
32. Yamada, T.; Kawai, M.; Wawro, A.; Suto, S.; Kasuya, A. HREELS, STM, and STS study of CH_3-Terminated Si(111)-(1 x 1) Surface. *J. Chem. Phys.* **2004**, *121*, 10660-10667.
33. Yu, H.; Webb, L. J.; Ries, R. S.; Solares, S. D.; Goddard, W. A.; Heath, J. R.; Lewis, N. S. Low-Temperature STM Images of Methyl-Terminated Si(111) Surfaces. *J. Phys. Chem. B* **2004**, *109*, 671-674.
34. O’Leary, L. E.; Johansson, E.; Brunschwig, B. S.; Lewis, N. S. Synthesis and Characterization of Mixed Methyl/Allyl Monolayers on Si(111). *J. Phys. Chem. B* **2010**, *114*, 14298-14302.

35. Hurley, P. T.; Nemanick, E. J.; Brunschwig, B. S.; Lewis, N. S. Covalent Attachment of Acetylene and Methylacetylene Functionality to Si(111) Surfaces: Scaffolds for Organic Surface Functionalization while Retaining Si−C Passivation of Si(111) Surface Sites. *J. Am. Chem. Soc.* **2006**, *128*, 9990-9991.
36. Puniredd, S. R.; Assad, O.; Haick, H. Highly Stable Organic Monolayers for Reacting Silicon with Further Functionalities: The Effect of the C−C Bond nearest the Silicon Surface. *J. Am. Chem. Soc.* **2008**, *130*, 13727-13734.
37. Assad, O.; Puniredd, S. R.; Stelzner, T.; Christiansen, S.; Haick, H. Stable Scaffolds for Reacting Si Nanowires with Further Organic Functionalities while Preserving Si−C Passivation of Surface Sites. *J. Am. Chem. Soc.* **2008**, *130*, 17670-17671.
38. Puniredd, S. R.; Assad, O.; Haick, H. Highly Stable Organic Modification of Si(111) Surfaces: Towards Reacting Si with Further Functionalities while Preserving the Desirable Chemical Properties of Full Si−C Atop Site Terminations. *J. Am. Chem. Soc.* **2008**, *130*, 9184-9185.
39. Yang, F.; Hunger, R.; Roodenko, K.; Hinrichs, K.; Rademann, K.; Rappich, J. Vibrational and Electronic Characterization of Ethynyl Derivatives Grafted onto Hydrogenated Si(111) Surfaces. *Langmuir* **2009**, *25*, 9313-9318.
40. Briggs, D.; Seah, M. P. *Practical Surface Analysis: Auger and X-ray Photoelectron Spectroscopy*, 2nd ed.; John Wiley & Sons, Inc.: New York, 1990; Vol. 1.
41. Haber, J. A.; Lewis, N. S. Infrared and X-ray Photoelectron Spectroscopic Studies of the Reactions of Hydrogen-Terminated Crystalline Si(111) and Si(100) Surfaces with Br_2, I_2, and Ferrocenium in Alcohol Solvents. *J. Phys. Chem. B* **2002**, *106*, 3639-3656.

42. van der Marel, C.; Yildirim, M.; Stapert, H. R. Multilayer Approach to the Quantitative Analysis of X-ray Photoelectron Spectroscopy Results: Applications to Ultrathin SiO_2 on Si and to Self-Assembled Monolayers on Gold. *J. Vac. Sci. Technol. A* **2005**, *23*, 1456-1470.
43. Seah, M. P.; Spencer, S. J. Ultrathin SiO_2 on Si II. Issues in Quantification of the Oxide Thickness. *Surf. Interface Anal.* **2002**, *33*, 640-652.
44. Yablonovitch, E.; Allara, D. L.; Chang, C. C.; Gmitter, T.; Bright, T. B. Unusually Low Surface-Recombination Velocity on Silicon and Germanium Surfaces. *Phys. Rev. Lett.* **1986**, *57*, 249-252.
45. Jaeckel, B.; Hunger, R.; Webb, L. J.; Jaegermann, W.; Lewis, N. S. High-Resolution Synchrotron Photoemission Studies of the Electronic Structure and Thermal Stability of CH_3- and C_2H_5-Functionalized Si(111) Surfaces. *J. Phys. Chem. C* **2007**, *111*, 18204-18213.
46. Contarini, S.; Howlett, S. P.; Rizzo, C.; De Angelis, B. A. XPS Study on the Dispersion of Carbon Additives in Silicon Carbide Powders. *Appl. Surf. Sci.* **1991**, *51*, 177-183.
47. Muehlhoff, L.; Choyke, W. J.; Bozack, M. J.; Yates, J. T. Comparative Electron Spectroscopic Studies of Surface Segregation on SiC(0001) and SiC(000$\bar{1}$). *J. Appl. Phys.* **1986**, *60*, 2842-2853.
48. Becker, R. S.; Golovchenko, J. A.; McRae, E. G.; Swartzentruber, B. S. Tunneling Images of Atomic Steps on the Si(111)7x7 Surface. *Phys. Rev. Lett.* **1985**, *55*, 2028-2031.

49. Ferguson, G. A.; Raghavachari, K. Collective Vibrations in Cluster Models for Semiconductor Surfaces: Vibrational Spectra of Acetylenyl and Methylacetylenyl Functionalized Si(111). *J. Chem. Phys.* **2007**, *127*, 194706.
50. Boyd, D. R. J.; Thompson, H. W. The Infra-Red Spectrum of Methyl Acetylene. *T. Faraday Soc.* **1952**, *48*, 493-501.
51. Kondo, S.; Koga, Y. Infrared Absorption Intensities of Methyl Acetylene. *J. Chem. Phys.* **1978**, *69*, 4022-4031.
52. Wong, K. T.; Kim, Y.-G.; Soriaga, M. P.; Brunschwig, B. S.; Lewis, N. S. Synthesis and Characterization of Atomically Flat Methyl-Terminated Ge(111) Surfaces. *J. Am. Chem. Soc.* **2015**.
53. Hunger, R.; Fritsche, R.; Jaeckel, B.; Jaegermann, W.; Webb, L. J.; Lewis, N. S. Chemical and Electronic Characterization of Methyl-Terminated Si(111) Surfaces by High-Resolution Synchrotron Photoelectron Spectroscopy. *Phys. Rev. B* **2005**, *72*, 045317.